RSC Advances

ROYAL SOCIETY OF CHEMISTRY

www.rsc.org/advances

Silver@Graphene Oxide Nanocomposite-Based Optical Sensor Platform for Biomolecules

Khosro Zangeneh Kamali, Alagarsamy Pandikumar, Gandhi Sivaraman, Hong Ngee Lim, Stephen Paul Wren, Tong Sun, Nay Ming Huang

Graphical Abstract

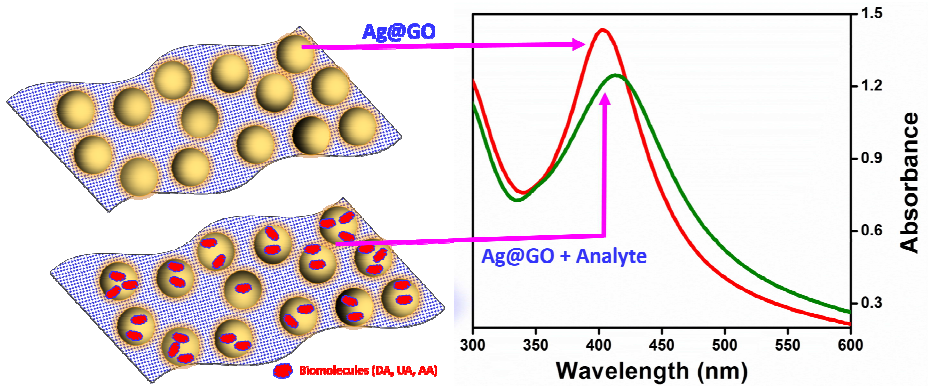

Silver incorporated graphene oxide nanocomposite prepared and used for the detection of biomolecules using absorbance based optical sensing method.

Silver@Graphene Oxide Nanocomposite-Based Optical Sensor Platform for Biomolecules

Khosro Zangeneh Kamali,[1] Alagarsamy Pandikumar,[1*] Gandhi Sivaraman,[2] Hong Ngee Lim,[3] Stephen Paul Wren,[4] Tong Sun,[4] Nay Ming Huang [1*]

[1] Low Dimensional Materials Research Centre, Department of Physics, Faculty of Science, University of Malaya, 50603 Kuala Lumpur, Malaysia.

[2]School of Chemistry, Madurai Kamaraj University, Madurai-625021, India.

[3] Department of Chemistry, Faculty of Science, Universiti Putra Malaysia, 43400 UPM Serdang, Selangor, Malaysia.

[4]School of Engineering and Mathematical Sciences, City University London, London EC1V0HB, United Kingdom.

Corresponding author's: huangnayming@um.edu.my.com (Nay Ming Huang), pandikumarinbox@gmail.com (Alagarsamy Pandikumar),

Abstract

In this report, a silver@graphene oxide (Ag@GO) nanocomposite-based optical sensor was developed for the detection of biomolecules such as dopamine (DA), ascorbic acid (AA), and uric acid (UA). An aqueous solution of Ag@GO was prepared using a simple chemical reduction method, and it showed a characteristic surface plasmon resonance (SPR) band at 402 nm. The SPR features of the Ag@GO nanocomposite were used for the detection of DA, AA, and UA. The SPR intensity-based limits of detection (LODs) of DA, AA, and UA were 49 nM, 634 nM, and 927 nM, respectively. The SPR band position-based LODs of DA, AA, and UA were 30 nM, 1.64 μM, and 2.15 μM, respectively. The present optical sensor was more sensitive to DA than to UA and AA. The interactions of the biomolecules with Ag@GO were studied based on the density functional theory (DFT), and it was found that DA had more interaction than AA and UA. This novel Ag@GO nanocomposite is simple to prepare and showed excellent stability and sensitivity toward the detection of biomolecules.

Keywords: Silver Nanoparticles; Graphene; Optical Sensor; Biosensor; Biomolecules

1. Introduction

For several decades, silver (Ag) nanoparticles have been attracting attention because of their excellent optical and electronic properties, high catalytic activity, and biocompatibility. Hence, they are used in a wide range of applications such as catalysis [1], solar cells [2,3], and optical [4] and electrochemical sensors [5]. Ag nanoparticles possess a sharp absorption in the visible region (400–500 nm), depending on the size of the nanoparticles. This absorption feature arises from the surface plasmon resonance (SPR), which is the absorption of light by the nanoparticles because of surface vibrations between atoms [6–8]. This SPR feature allows Ag nanoparticles to be used in optical sensors for the detection of toxic metals [9], biomolecules [10], and organic compounds[11]. The addition of any analyte to the Ag nanoparticles leads to assembled/aggregated nanoparticles. This influences the SPR absorption band and is extensively used to follow the molecular recognition processes.

Dopamine (DA) is an important catecholamine that belongs to the family of excitatory chemical neurotransmitters. It plays an essential role in the functioning of the drug addiction, cardiovascular, renal, central nervous, and hormonal systems, and in Parkinson's disease [12]. Thus, it is very important to develop a simple sensor for the detection of a sub-micro-molar concentration of DA. In recent years, the detection of biomolecules such as uric acid (UA) and ascorbic acid (AA) in human fluids such as urine and serum has gained considerable attention [13]. A deficiency or excess amount of UA in the body causes several diseases, including Lesch/Nyhan syndrome, hyperuricaemia, and gout [14]. Cardiovascular disease and kidney damage result from an elevated UA concentration in serum [15]. Analytical methods such as high-performance liquid chromatography (HPLC) [16], spectrofluorimetry [17], spectrophotometry [18],

mass spectrometry [19], and electrochemical sensors [20] have been reported for the detection of these neurotransmitter molecules. However, the existing detection methods have several limitations such as the need for expensive equipment, well-trained operators, and tedious sampling and time-consuming procedures. Alternatively, an optical sensor platform is more attractive for sensing a wide range of analytes. It is cost effective, portable, has a rapid response, and can provide real-time analyses. Recently, Ramaraj and his coworker reported a silicate-Ag nanoparticle-based optical sensor for the detection of DA, UA, and AA with LODs of 5, 5, and 1 nM, respectively [9] (**Scheme 1**).

Most commonly, Ag nanoparticles are synthesized using various chemical and physical methods, which are not eco-friendly and suffer from problems that include the poor reproducibility and stability of the Ag nanoparticles due to colloidal aggregation [21]. In order to overcome such limitations, considerable efforts have been made to prepare Ag nanoparticles on polymer [22], silicate sol-gel [11], and graphene nanosheets [23]. Among these, Ag-graphene has a large surface area and strong van der Waals force between the graphene and Ag nanoparticles, which significantly reduces nanoparticle aggregation. In addition, the high interfacial interactions ensure the stability of the Ag nanoparticles [24]. In this study, graphene oxide-supported Ag nanoparticles were prepared using a simple chemical reduction method and used in an optical sensor for the detection of biomolecules such as DA, AA, and UA (**Scheme 2**). The present synthetic method for the for preparation of Ag@GO nanocomposite has advantages over other methods[11,21-24] such as, long term stability, high homogeneity, rapid and ease of preparation and avoids any surfactant, stabilizers.

2. Experimental Methods

2.1. Chemicals and Reagents

Graphite flakes were purchased from Ashbury Inc. USA. Chemical reagents such as silver nitrate ($AgNO_3$), sulphuric acid (H_2SO_4, 98%), phosphoric acid (H_3PO_4, 85%), potassium permanganate ($KMnO_4$, 99.9%), hydrogen peroxide (H_2O_2, 30%), 3-hydroxytyraminium chloride (dopamine, DA), L(+)-ascorbic acid (AA), and uric acid (UA) were purchased from Merck. Sodium borohydride ($NaBH_4$) was received from Systerm. All the other chemicals used were of analytical grade and used without further purification. All the solutions were prepared using deionized water.

2.2. Preparation of Ag@GO Nanocomposite

The Ag@GO nanocomposite was prepared as follows. Initially, GO was prepared by following the well-known simplified Hummer's method [25]. A 4 mg quantity of GO was dispersed in 30 mL of DI water. Then, 85 mg of silver nitrate ($AgNO_3$) was separately dissolved in 10 mL of DI water and mixed with the GO solution, after which the mixture solution was sonicated for 15 min at 50 W using a horn sonicator in order to homogeneously mix Ag^+ ions on GO surface and break GO sheets into smaller pieces in a cool bath. At the end of the sonication, 400 μL of 5 mM of freshly prepared sodium borohydride ($NaBH_4$) solution was added to the GO-$AgNO_3$ solution. After this addition, the color of the solution instantly became dark yellow as a result of the formation of silver nanoparticles. The prepared Ag@GO nanocomposite was mixed with 30 mL of DI water and stored in a vial without any washing or purification.

2.3. Characterization Techniques

The morphologies of the prepared Ag@GO nanocomposite with and without biomolecules were examined using a JEOL JEM-2100 F high-resolution transmission electron microscope. The optical absorption in the spectral region of 190–900 nm was assessed using a Thermo Scientific Evolution 300 UV-vis spectrophotometer. The Raman spectra were collected using a Renishaw 2000 inVia system with an argon ion laser emitting at 532 nm.

2.4. Optical Detection of Biomolecules

The optical sensing of biomolecules, including DA, AA, and UA, using the Ag@GO nanocomposite was performed using the Thermo Scientific Evolution 300 UV-vis absorption spectrophotometer. The absorption spectra of the Ag@GO nanocomposite were recorded upon the addition of various biomolecule contents such as DA, AA, and UA. For the optical detection, 10 μM of optimized analyte concentration (DA/AA/UA) was added into 2 mL of the Ag@GO solution, shaken well, and subjected to a constant resting time. The absorbance spectra of Ag@GO solution with the addition of different concentration of analyte were recorded. Then, the difference in the absorbance was monitored by recording the absorbance spectrum.

3. Results and Discussion

The absorbance spectra of the $AgNO_3$, GO, and synthesized Ag@GO nanocomposite are shown in **Fig. 1**. The peak at 265 nm for $AgNO_3$ corresponds to the absorbance peak of Ag^+ ions [26,27]. The visible peak at 230 and a shoulder at 300 nm in the GO absorbance spectrum are attributed to the $\pi \rightarrow \pi^*$ of the aromatic C–C bond and the $n \rightarrow \pi^*$ of the C=O bond transition, respectively [28]. The addition of $NaBH_4$ to the GO-$AgNO_3$ solution caused a reduction in the Ag^+

ions into Ag^0 and resulted in the formation of Ag nanoparticles on the GO. The existence of the n→π* transition of the C=O bond (absorbance at 300 nm) after the addition of $NaBH_4$ to the GO-$AgNO_3$ solution suggested that $NaBH_4$ produced a reduction in the Ag ions to Ag nanoparticles, but did not reduce the GO to rGO.

3.2. Optical Sensing of Biomolecules using Ag@GO Nanocomposite

The biomolecule sensing abilities of Ag@GO were investigated in absorbance-based titration experiments with different concentrations of the analytes (DA, AA and UA). The changes in the SPR band intensity and peak position of the Ag@GO nanocomposite were used for the sensing of the biomolecules. The absorbance of the Ag@GO sample recorded by the titration of DA with a concentration range of 100 nM up to 2 μM at intervals is shown in **Fig. 2**, along with the obtained absorbance changes by this titration. **Fig. 2A** shows the decrease in the absorption intensity and red shift in the absorbance peak from increasing the concentration of dopamine in 100-nM steps. The decrease in the absorption and red shift in the absorption maximum can be explained by the Mie theory[29], which suggests that any changes in the refractive index of the local environment around the surface of noble metal nanoparticles will introduce some changes in the absorption intensity and/or position of the SPR absorption band. An increase in the refractive index usually produces a red shift to a longer wavelength in the SPR absorption band [10,29,30]. The changes in the absorption intensity and/or position of the SPR of the Ag@GO sample by the increasing concentration of dopamine are plotted in **Fig. 2(B and D)**. A linear relationship with a correlation coefficient of 0.9985 ($n = 20$) for the regression equation (λ_{shift} (nm) = 403 + 0.0065 nM) was obtained for the Ag@GO in the DA concentration range of

100 nm to 2 μM. The LOD was calculated to be 30 nM from the equation LOD = 3 × standard deviation of the regression line (σ)/slope (S).

Further, the decrease in the absorption intensity is plotted against the DA concentration (**Fig. 2B)**. It can be seen that the absorbance intensity of the Ag@GO nanocomposite decreased linearly upon the addition of DA in the concentration range of 100 nm–2 μM. **Fig. 2C** was plotted by assuming that I_d is the difference in the SPR absorption intensities of the Ag@GO nanocomposite in the absence and presence of DA at a given concentration. The decrease in the absorbance peak intensity follows two different linear proportional trends for a concentration below 1 μM and one of 1 to 2 μM. To make it easier to formulate the absorbance reduction, the absolute amount of reduction was calculated and plotted in **Fig. 2D**. In addition, two different linear segments were observed in the calibration plots of I_d versus the DA concentration, corresponding to two different ranges of substrate concentration. The correlation coefficient of 0.9966 (n = 10) for the regression equation I_d = 0.00409 + 7.45455E-5 nM was obtained for the Ag@GO in the DA concentration range of 100 nm to 1 μM, and the LOD was found to be 49 nM. The DA concentration range of 1 to 2 μM showed a correlation coefficient of 0.9991 (n = 10) for the regression equation I_d = -0.0315 + 1.08455E-4 nM, and the LOD was found to be 62 nM. Thus, the results indicated that Ag@GO is able to detect a very small amount of dopamine, ether by its reduction effect on its absorbance or/and red shift in the absorbance. A progressive increase in the DA concentration consequently decreased the absorption intensity and red shifted to a longer wavelength, due to the molecular bridging effects between the Ag nanoparticles and DA molecules.

Moreover, the addition of AA to the Ag@GO significantly influenced the SPR absorption features. The absorption spectra of Ag@GO with different AA concentrations are shown in **Fig. 3A**. The addition of AA to the Ag@GO decreased the absorbance intensity and also shifted the SPR maximum. Increasing the ascorbic acid to very high concentrations (more than 30 μM) caused a decrease in the pH of the solution, which led to a decrease in the surface charge of the GO sheets and the agglomeration of the Ag@GO nanocomposite [31]. This could be confirmed from the increased and broadened Ag peak in the absorption spectrum (Fig. 3A). The correlation coefficient of 0.9978 (n = 5) for the regression equation I_d = 0.00196 + 0.00928 μM was obtained for the Ag@GO in the AA concentration range of 5 to 30 μM, and the LOD was found to be 634 nM. Based on the SPR band shift, a correlation coefficient of 0.9977 (n = 5) for the regression equation λ_{shift} (nm) = 403 + 0.3038 μM was obtained, and the LOD was found to be 1.64 μM.

Fig. 4A shows the absorption spectra of Ag@GO with different UA concentrations. It can be seen that there was a decrease in the absorption intensity and red shift in the SPR band by increasing the concentration of UA in 5 μM additions. It can be observed that the intensity of the SPR band decreases gradually with an increase in the UA concentration, and it is accompanied by a slight red shift in the absorption maxima of the band, which is attributed to the partial oxidation of Ag nanoparticles [32]. The correlation coefficient of 0.9998 (n = 10) for the regression equation I_d = 0.00268+ 0.00254 μM was obtained for the Ag@GO in the UA concentration range of 5 to 50 μM, and the LOD was found to be 927 nM (**Fig. 4C**). Based on the SPR band shift, a correlation coefficient of 0.9973 (n = 10) for the regression equation λ_{shift} (nm) = 403 + 0.11 μM was obtained, and the LOD was found to be 2.15 μM (**Fig. 4D**).

The obtained results suggest that the carbonyl and amino groups present in UA and hydroxyl groups in AA and DA could interact with the Ag nanoparticles and influence the SPR band. The possible interactions of UA, AA, and DA with Ag nanoparticles were explored using computational studies (explained later), which suggested that the Ag nanoparticles prefer to bind with the N-site of DA molecules. Hence, the sensitivities and interaction strengths of the UA, AA, and DA on Ag@GO nanocomposite could be explained using the molar absorption coefficient values and SPR band position of the Ag@GO nanocomposite upon its interaction with the UA, AA, and DA.

The Ag@GO nanocomposite was further used to measure DA (2 μM), UA (5 μM) and AA (5 μM) in non-diluted human urine sample. A specified amount of standard DA, UA and AA were added, separately into urine sample. Table 1 depicts that the recovery of the urine sample containing 2.25, 5.45 and 5.63 μM are 112, 109 and 113 % for DA, UA and AA, respectively, indicating that the analytical procedures are free from the interferences in the urine sample. Several analytical methods used for the detection of biomolecules including electrochemical, SERS, and fluorescence method. Since each analytical methods have their own limitations. In the case of electrochemical method, fabrication of stable and reproducible sensor electrode is very difficult[33]. In fluorescence method, sensor materials must possess fluorescence property which is essential for the fluorimetric detection of biomolecules, if the property is absence in the sensor materials and this method cannot be used[34]**.** Other method reported for detection of biomolecules is surface-enhanced Raman scattering (SERS) and it is based on the interaction of groups on molecules between the sensor materials, however this method provides qualitative information

about the analytle but not a quantitative manner. Since the detection will be always carried out on the thin film and it may not have uniform distribution of sensor materials and analyte [35]. Present optical sensor possess merit such as very simple, easy to use, low-cost, ease of sample preparation and real time measurements in the detection of biomolecules when compared to the other analytical methods.

3.3. Morphological Studies of Ag@GO after Addition of Biomolecules

TEM images were recorded for the Ag@GO nanocomposite before and after the addition of AA, DA, and UA and are shown in **Fig. S1**. Upon the addition of UA and AA, the size of the Ag nanoparticles was decreased, which may have been due to the reducing effect of UA and AA on the Ag nanoparticles. However, even though UA and AA reduced the particle size, they could interact with the Ag nanoparticles and change their refractive index, which resulted in a red shift in their SPR absorbance peak. The other reason for the red shift in the SPR band of the Ag nanoparticles in the presence of AA and UA was the aggregation of the GO sheets due to the acidic media, because UA and AA are acidic in nature. On the other hand, the DA could not reduce the Ag nanoparticles, but it strongly interacted with the Ag nanoparticles through the amine group (Ag—NH_2) and caused aggregation of the Ag nanoparticles. It influenced the refractive index of the Ag nanoparticles and caused a change in the SPR band position and intensity [36]. The interaction between the DA and Ag nanoparticles was strong enough to bring the Ag NPs close to each other, which led to particle aggregation.

3.4. Raman Studies of Ag@GO Nanocomposite

Raman spectroscopy results for the pure Ag@GO and Ag@GO solutions containing 1 μM of DA, AA, and UA are shown in **Fig. S2**. Two major peaks are observed for all the samples at 1350 and 1590 cm^{-1}, which correspond to the D and G bands of graphene oxide, respectively. **Fig. S2a** shows that the pure Ag@GO sample does not have any peak for Ag nanoparticles. It can be seen from **Fig. S2(b-d)** that the addition of DA, UA, and AA to the Ag@GO composite leads to an increase in some of the Ag peaks and makes them more pronounced. This effect is due to enhancement in scattering of Ag particles in Ag@GO sample due to charge transfer (CT) and electromagnetic (EM) mechanism occurs after addition of analyte. The signal enhancement in electromagnetic mechanism is attributed to a strong amplification of the electromagnetic fields near the plasmon resonances of metal substrates after interaction of analyte with Ag NPs. Charge transfer mechanism is attributed to enhancement in Raman scattering of analyte molecules by electron transferred from SERS substrate to the neighbor molecule [37–39] . The higher abilities of AA and UA to transfer electrons are related to their higher reactivity compared to DA. The SERS method was used for tracing the amount of molecules, which is based on the increasing Raman intensity of noble metals in the presence of different amounts of investigated molecules [40–42]. The enhancement of SERS is attributed to electromagnetic field enhancement due to localized surface plasmon resonance (LSPR). The chemical interaction of Ag with the DA,UA, and AA causes easier electron transfer and also enhances the SERS [42,43]. The peaks at 460, 800, 950 and 1050 cm^{-1} were attributed to Ag nanoparticles; the observed enhancement was after addition of analytes [44,45]. Some reports state that SERS can occur by the interaction of the additive molecules and Ag nanoparticles [23,46–49].

3.5. Computational Studies

Molecular orbital (MO) study can be used to investigate the interaction force between Ag nanoparticles and analytes (DA, AA and UA). By examining the location of highest occupied molecular orbital (HOMO) and lowest unoccupied molecular orbital (LUMO) in the system, and the HOMO-LUMO energy gap, the affinity pattern of the molecules can be determined. In order to account for the changes in the photophysical properties of Ag nanoparticles interacting with UA, AA, and DA, DFT-B3LYP/LANL2DZ level calculations were carried out using the Gaussian 09 program[49]. The UA, AA, and DA were optimized on the Ag nano-array substrates, and DFT B3LYP/LANL2DZ basis sets and their absorption behavior from the optimized structures were calculated using time dependent density functional theory (TDDFT) calculations with the above-mentioned sets. The lowest energy minimized structures for the Ag nanoparticles with DA, UA, and AA are shown in **Fig. 5** The electron density separation for the HOMO and LUMO are shown in **Fig. 5** for DA, UA, and AA, and it is observed that the HOMO resided mainly on the silver clusters. In the Ag–DA adduct, LUMO is located on the dopamine molecule, whereas in the Ag–UA, the corresponding LUMO population is located mainly on the uric acid group, as well as the Ag clusters. In Ag-AA, LUMO is found on silver clusters with little contribution from the AA moiety. The HOMO–LUMO energy separation has been used as a simple indicator of kinetic stability and could indicate the affinity pattern of the molecule. A reasonable HOMO–LUMO energy gap (3.8214 eV for Ag-DA, 3.9220 eV for Ag-UA, and 3.9293 eV for Ag-AA) showing that the reasonably high affinity for DA with Ag and lower affinity for UA and AA agree with the fact that it is energetically unfavorable to add electrons to a high-lying LUMO or to extract electrons from a low-lying LUMO. The simulated spectra of the Ag nanoparticles with DA, UA, and AA obtained from the TD-DFT calculations concur with

the experimental absorption spectra. Hence, it is clear that the changes in the SPR responses of Ag nanoparticle clusters with DA, UA, and AA due to the binding of these species lead to the formation of an internal charge transfer (ICT) complex. DFT studies gave further evidence for the higher detection limit of DA due to the higher binding with Ag nanoparticles compared to the others, as confirmed by the energy gap [49].

4. Conclusions

In the present study, we demonstrated a facile method for the synthesis of a Ag@GO nanocomposite via the chemical reduction of Ag ions in the presence of GO. The graphene oxide stabilized the Ag nanoparticles in an aqueous solution and prevented the aggregation of these particles. The nanocomposite showed an SPR band at 402 nm due to the Ag nanoparticles. An SPR-based optical sensor was developed with Ag@GO for the detection of DA, UA, and AA. This SPR-based optical sensor showed a very high sensitivity without requiring tedious pretreatment and the use of expensive devices. The selectivity of this nanocomposite was also investigated using other biological molecules, AA and UA. The SPR absorbance peak changes toward UA and AA were not comparable with DA, which proved its excellent selectivity. The SPR intensity-based LODs of DA, AA, and UA were 49 nM, 697 nM, and 927 nM, respectively. The SPR band position-based LODs of DA, AA, and UA were 30 nM, 1.64 μM, and 2.15 μM, respectively. The adsorption and sensing ability of the Ag@GO nanocomposite mainly depended on the nature of the adsorption site and its interaction with the functional groups of the molecules, along with the aggregation of GO in an acidic solution. Further, DFT studies proved that DA had more affinity with Ag@GO than UA and DA. This approach can be applied to

design and optimize SPR-based chemical and biological nanosensors for the detection of other biomolecules.

Acknowledgements

The current research work was supported by a University of Malaya Research Grant, UMRG Program (RP007C-13AFR), and a High Impact Research Grant from the Ministry of Higher Education of Malaysia (UM.C/625/1/HIR/MOHE/SC/21).

References

1. X. Yang, A. Zhang, G. Gao, D. Han, C. Han, J. Wang, H. Lu, J. Liu and M. Tong, *Catal. Commun.*, 2014, **43**, 192–196.
2. S. Lim, N. Huang, H. Lim and M. Mazhar, *Int. J. Photoenergy*, 2014, **2014**.
3. A. Pandikumar, K. M. Saranya and R. Ramaraj, *Appl. Phys. Lett.*, 2012, **101**, 093112.
4. P. Rameshkumar, S. Manivannan and R. Ramaraj, *J. Nanopart. Res.*, 2013, **15**, 1639.
5. A. Moradi Golsheikh, N. M. Huang, H. N. Lim, R. Zakaria and C.-Y. Yin, *Carbon N. Y.*, 2013, **62**, 405–412.
6. K. L. Kelly, E. Coronado, L. L. Zhao and G. C. Schatz, *J. Phys. Chem. B*, 2003, **107**, 668–677.
7. M.-C. Daniel and D. Astruc, *Chem. Rev.*, 2004, **104**, 293–346.
8. S. Jayabal, R. Sathiyamurthi and R. Ramaraj, *J. Mater. Chem. A*, 2014, **2**, 8918.
9. G. Maduraiveeran and R. Ramaraj, *J. Anal. Chem.*, 2013, **68**, 241–248.
10. G. Maduraiveeran and R. Ramaraj, *J. Nanopart. Res.*, 2011, **13**, 4267–4276.
11. G. Maduraiveeran and R. Ramaraj, *Anal. Chem.*, 2009, **81**, 7552–7560.
12. D. P. Nikolelis, D. a Drivelos, M. G. Simantiraki and S. Koinis, *Anal. Chem.*, 2004, **76**, 2174–80.

13. S. R. Ali, R. R. Parajuli, Y. Ma, Y. Balogun and H. He, *J. Phys. Chem. B*, 2007, **111**, 12275–81.

14. H. A. Harper, *Review of physiological chemistry*, Lange Medical Publications, Los Altos, CA, 13th ed., 1977.

15. M. Mazzali, J. Hughes, Y. G. Kim, J. A. Jefferson, D. H. Kang, K. L. Gordon, H. Y. Lan, S. Kivlighn and R. J. Johnson, *J. Hypertens.*, 2001, **13**, 324.

16. J. M. Wilson, J. T. Slattery, A. J. Forte and S. D. Nelson, *J Chromatogr*, 1982, **227**, 453–462.

17. H. Y. Wang, Y. Sun and B. Tang, *Talanta*, 2002, **57**, 899–907.

18. M. Mamiński, M. Olejniczak, M. Chudy, A. Dybko and Z. Brzózka, *Anal. Chim. Acta*, 2005, **540**, 153–157.

19. H. C. Curtius, M. Wolfensberger, B. Steinmann, U. Redweik and J. Siegfried, *J. Chromatogr. A*, 1974, **99**, 529–540.

20. G. Thien Soon How, A. Pandikumar, N. M. Huang and H. N. Lim, *Sci. Rep.*, 2014, **4**, 5044.

21. U. Nickel, A. zu Castell, K. Pöppl and S. Schneider, *Langmuir*, 2000, 9087–9091.

22. J. Lu, K.-S. Moon and C. P. Wong, *J. Mater. Chem.*, 2008, **18**, 4821.

23. S. V. Kumar, N. M. Huang, H. N. Lim, M. Zainy, I. Harrison and C. H. Chia, *Sens. actuat b-chem*, 2013, **181**, 885–893.

24. H. Zhao, H. Fu, C. Tian, Z. Ren and G. Tian, *J. Colloid Interface Sci.*, 2010, **351**, 343–347.

25. N. M. Huang, H. N. Lim, C. H. Chia, M. a Yarmo and M. R. Muhamad, *Int. J. Nanomedicine*, 2011, **6**, 3443–8.

26. S. Sharma, P. Sanpui, A. Chattopadhyay and S. S. Ghosh, *RSC Adv.*, 2012, **2**, 5837.

27. T. Peter Amaladhas, S. Sivagami, T. Akkini Devi, N. Ananthi and S. Priya Velammal, *Adv. Nat. Sci. Nanosci. Nanotechno*, 2012, **3**, 045006.

28. J. I. Paredes, S. Villar-Rodil, A. Martínez-Alonso and J. M. D. Tascón, *Langmuir*, 2008, **24**, 10560–4.

29. C. F. Bohren and D. R. Huffman, *Absorption and scattering of light by small particles*, Wiley, Newyork, 1983.

30. T. Balaji, M. Sasidharan and H. Matsunaga, *Analyst*, 2005, **130**, 1162–1167.

31. X. Hu, Y. Yu, W. Hou, J. Zhou and L. Song, *Appl. Surf. Sci.*, 2013, **273**, 118–121.

32. N. Misra, V. Kumar, L. Borde and L. Varshney, *Sens. Actuators B Chem*, 2013, **178**, 371–378.

33. B. Kaur, T. Pandiyan, B. Satpati and R. Srivastava, *Colloids Surf. B. Biointerfaces*, 2013, **111C**, 97–106.

34. Y. Lin, M. Yin, F. Pu, J. Ren and X. Qu, *Small*, 2011, **7**, 1557–1561.

35. B. Yanru and L. Sang-Wha, *J. Nanosci. Nanotechnol.*, 2013, **13**, 5992–5996.

36. R. Desai, V. Mankad, S. K. Gupta and P. K. Jha, *J. Nanosci. Nanotechnol. lett.*, 2012, **4**, 30–34.

37. A. Otto, *J. Raman Spectrosc.*, 1991, **22**, 743–752.

38. G. Brolo and E. Donald, 1997, **405**, 29–44.

39. P. Kambhampati and A. Campion, 1999, **428**, 115–125.

40. A. Campion, P. Kambhampati and C. Harris, *Chem. Soc. Rev.*, 1998, **27**, 241–250.

41. I. Pavel, E. McCarney and A. Elkhaled, *J. Phys. Chem. C Nanomater Interfaces.*, 2008, **112**, 4880–4883.

42. K. Kneipp, Y. Wang, H. Kneipp, L. Perelman, I. Itzkan, R. Dasari and M. Feld, *Phys. Rev. Lett.*, 1997, **78**, 1667–1670.

43. M. Hankus, H. Li, G. Gibson and B. Cullum, *Anal. Chem.*, 2006, **78**, 7535–7546.

44. X. Zou, E. Ying and S. Dong, *J. Colloid Interface Sci.*, 2007, **306**, 307–15.

45. R. F. Aroca, R. a Alvarez-Puebla, N. Pieczonka, S. Sanchez-Cortez and J. V Garcia-Ramos, *Adv. Colloid Interface Sci.*, 2005, **116**, 45–61.

46. Y. Bu and S. Lee, *ACS Appl. Mater. Interfaces*, 2012, **4**, 3923–31.

47. D. a Stuart, C. R. Yonzon, X. Zhang, O. Lyandres, N. C. Shah, M. R. Glucksberg, J. T. Walsh and R. P. Van Duyne, *Anal. Chem.*, 2005, **77**, 4013–4019.

48. L. Zhou, H. Gu, C. Wang, J. Zhang, M. Lv and R. He, *Colloids Surf., A*, 2013, **430**, 103–109.

49. M. Culha, B. Cullum, N. Lavrik and C. K. Klutse, *J. Nanotechnol.*, 2012, **2012**, 971380.

50. M. J. Frisch, G. W. Trucks, H. B. Schlegel, G. E. Scuseria,M. A. Robb, J. R. Cheeseman, G. Scalmani, V. Barone,B. Mennucci, G. A. Petersson, H. Nakatsuji, M. Caricato,X. Li, H. P. Hratchian, A. F. Izmaylov, J. Bloino, G. Zheng, J. L. Sonnenberg, M. Hada, M. Ehara, K. Toyota, R. Fukuda, J. Hasegawa, M. Ishida, T. Nakajima, Y. Honda,O. Kitao, H. Nakai, T. Vreven, J. A. Montgomery, Jr, J. E. Peralta, F. Ogliaro, M. Bearpark, J. J. Heyd, E. Brothers, K. N. Kudin, V. N. Staroverov, R. Kobayashi, J. Normand, K. Raghavachari, A. Rendell, J. C. Burant, S. S. Iyengar, J. Tomasi, M. Cossi, N. Rega, J. M. Millam, M. Klene, J. E. Knox, J. B. Cross, V. Bakken, C. Adamo, J. Jaramillo, R. Gomperts, R. E. Stratmann, O. Yazyev, A. J. Austin, R. Cammi, C. Pomelli, J. W. Ochterski, R. L. Martin, K. Morokuma, V. G. Zakrzewski, G. A. Voth, P. Salvador, J. J. Dannenberg, S. Dapprich, A. D. Daniels, O. Farkas, J. B. Foresman, J. V. Ortiz, J. Cioslowski and D. J. Fox, Gaussian 09, Revision A.02, Gaussian, Inc., Wallingford CT, 2009.

Figures and caption

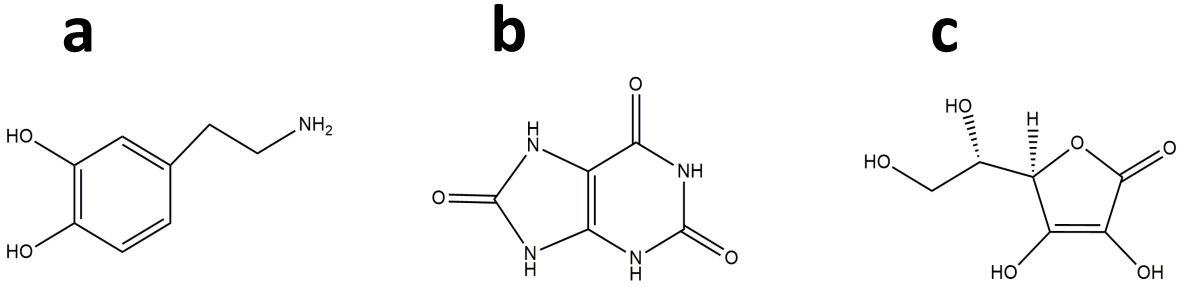

Scheme 1. Molecular structure of (a) dopamine, (b) uric acid and, (c) ascorbic acid.

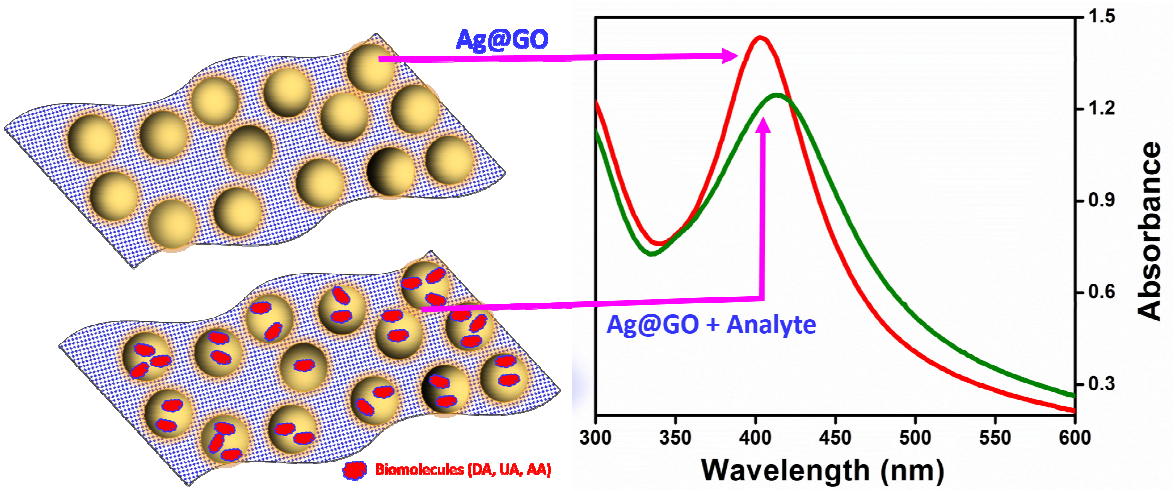

Scheme 2. Schematic representation of optical sensing of biomolecules with Ag@GO nanocomposite.

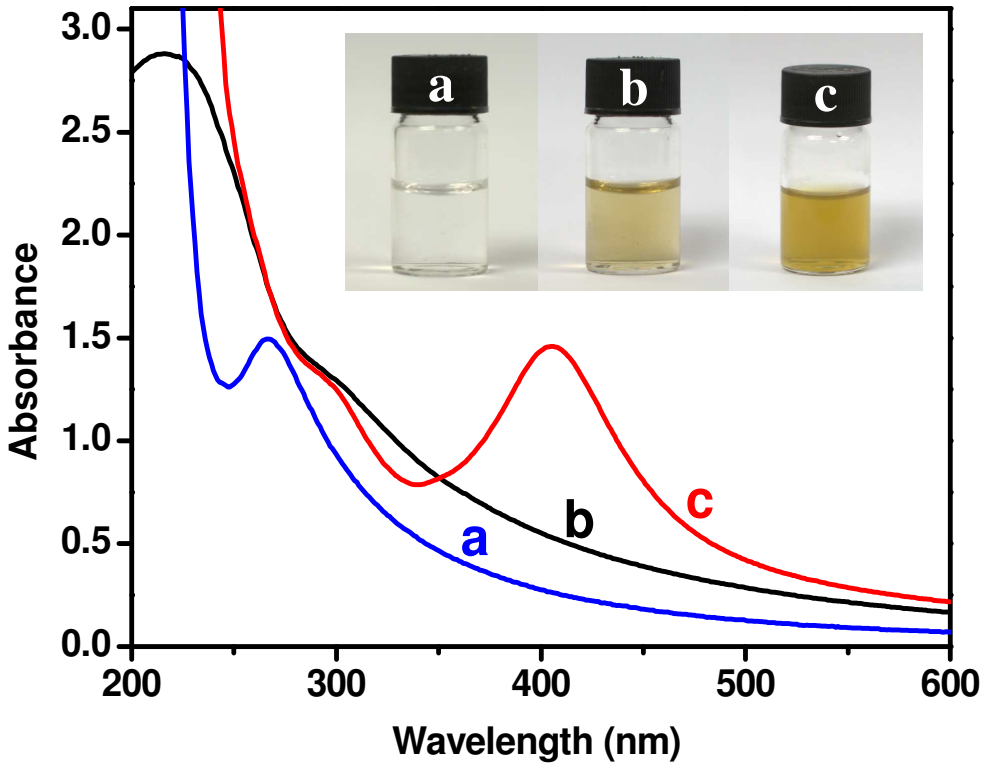

Fig. 1: UV-vis absorption spectra of (a) $AgNO_3$ (b) GO, and (c) Ag@GO nanocomposite. **Inset:** Photograph obtained for the aqueous solution of synthesized Ag@GO nanocomposite.

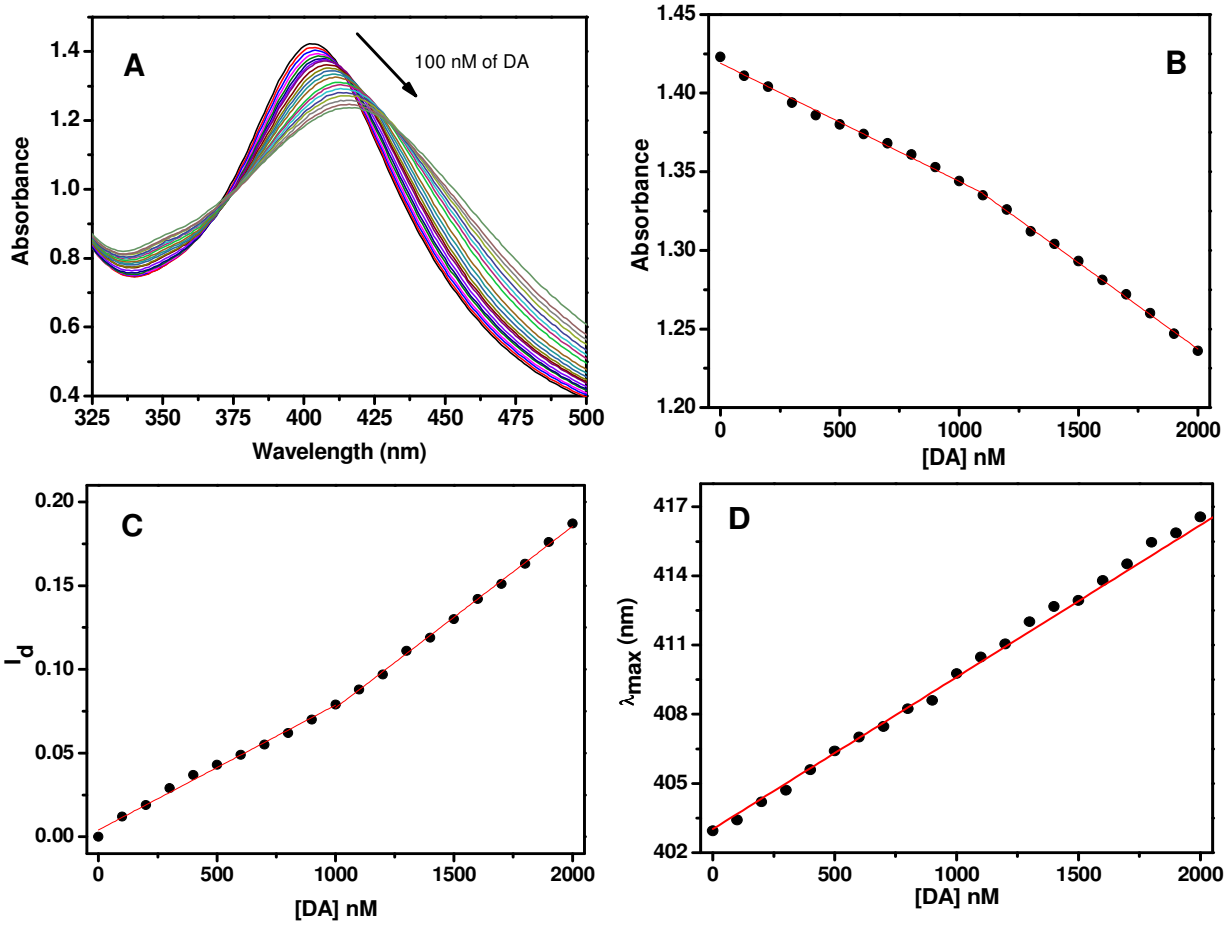

Fig. 2: (A) Absorption spectra obtained for Ag@GO nanocomposite upon each addition of 100 nM DA. (B) Plot of absorption intensity *vs.* DA concentration. (C) Plot of I_d *vs.* DA concentration. (D) Plot of λ_{max} *vs*. DA concentration.

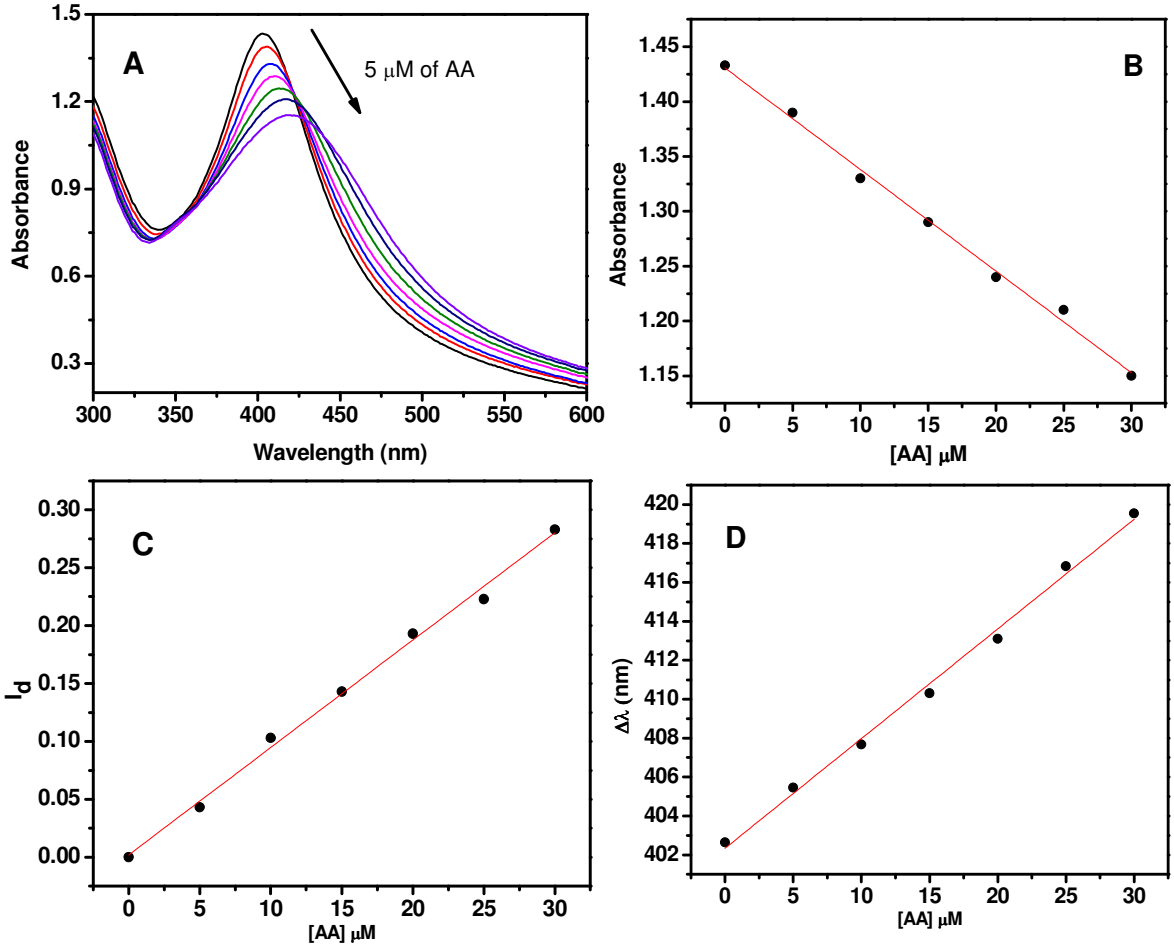

Fig. 3: (A) Absorption spectra obtained for Ag@GO nanocomposite upon each addition of 5 μM AA. (B) Plot of absorption intensity *vs.* AA concentration. (C) Plot of I_d *vs.* AA concentration. (D) Plot of λ_{max} *vs*. AA concentration.

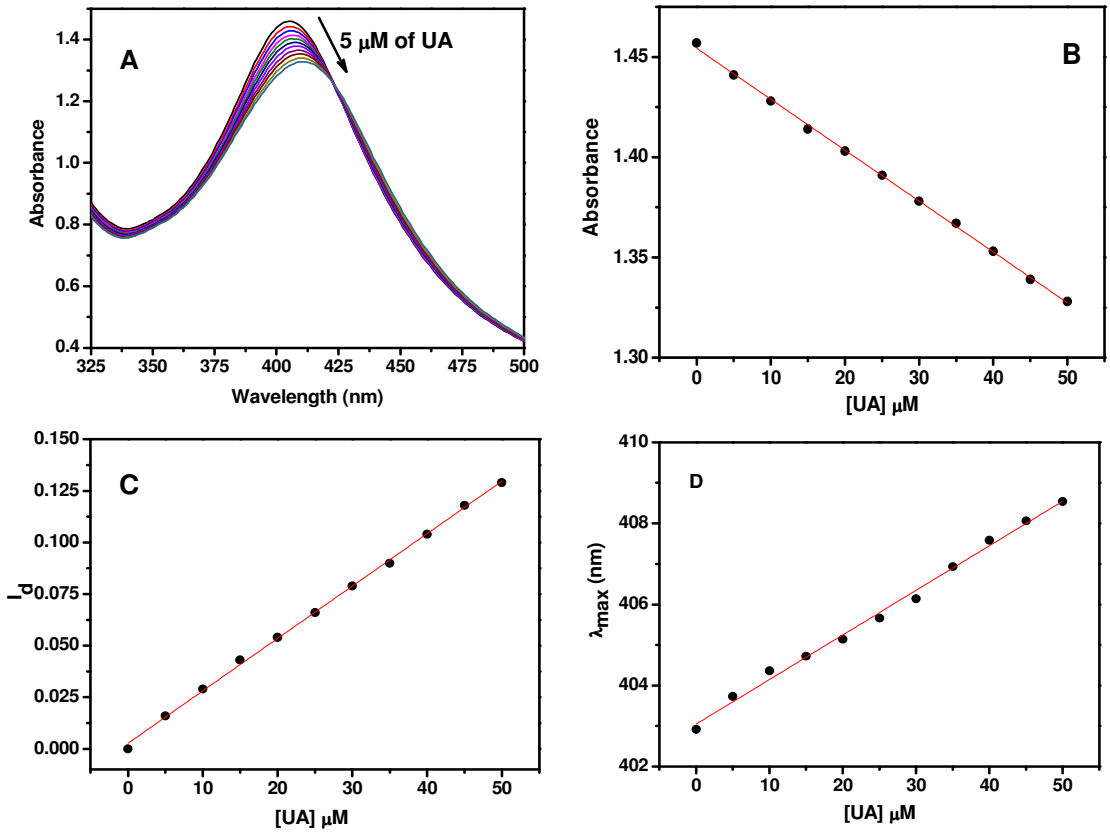

Fig. 4: (A) Absorption spectra obtained for Ag@GO nanocomposite upon each addition of 5 μM UA. (B) Plot of absorption intensity *vs.* UA concentration. (C) Plot of I_d *vs.* UA concentration. (D) Plot of λ_{max} *vs*. UA concentration.

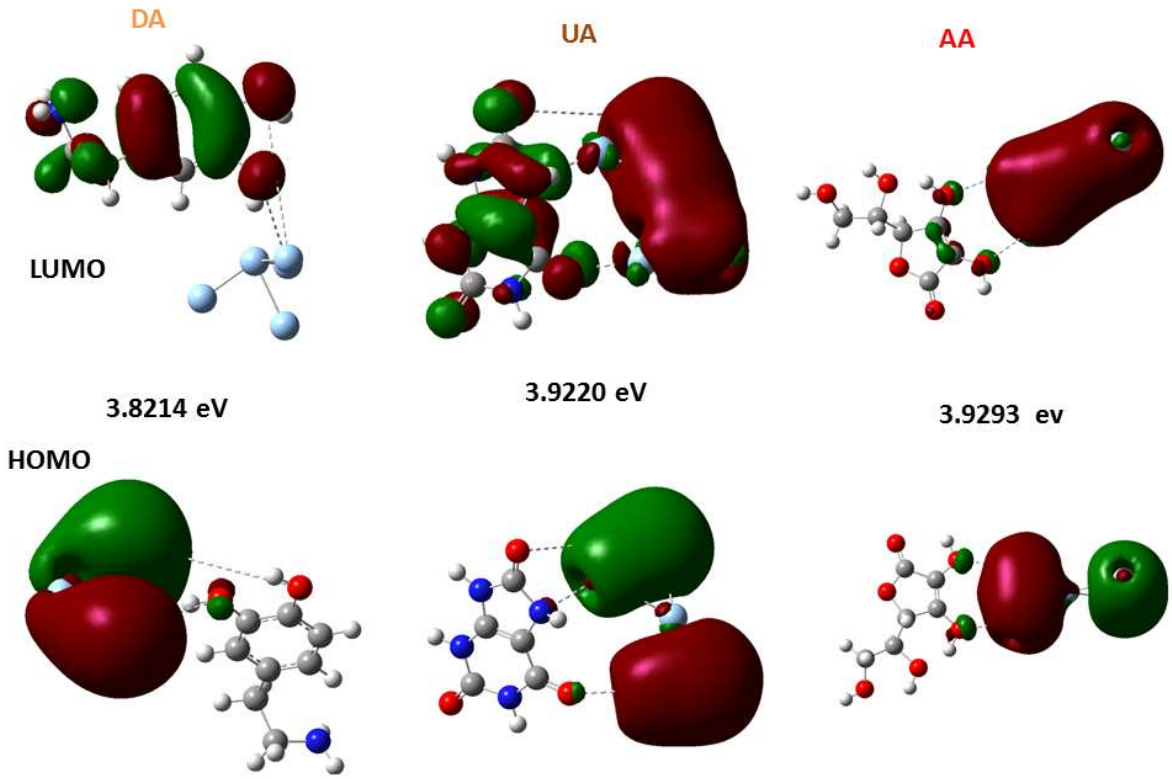

Fig. 5: Electron density map and energy gap of HOMO and LUMO energy levels for Ag and DA, UA, and AA adducts, respectively calculated by DFT methods.

Table

Table 1: Analytical performances of Ag@GO nanocomposite for the detection of DA, UA and AA in human urine sample.

Analyte	Spiked (µM)	Found (µM)	*Recovery (%)
DA	2	2.25	112
UA	5	5.45	109
AA	5	5.63	113

***Recovery = (C_{Found}/C_{Sipked}) × 100.**